https://doi.org/10.21289/KSIC.2022.25.4.505

Optimized Location Selection of Active Mounting System Applied to 1D Beam Structure

Byeongil Kim[1*]

〈Abstract〉

The objective of this article is finding optimized locations of active mounts applied to 6-DOF beam structure with two active paths. When sinusoidal excitation forces are applied to the beam structure, secondary forces from two active mounts which can minimize (ideally becoming zero) transmitted forces are calculated mathematically and the vibration attenuation performance is validated through computer simulations. When the force applied to two active mounts are relatively low, those specific locations are considered as optimized location of active mounting system. As the location of mount changes, amplitude and phase of secondary forces in each path are analyzed with 3D plots. Based on the simulation results, a criterion for selecting mounting location is suggested and it would be very useful for selecting actuators for active mounts appropriately.

Keywords : Location Criteria, Piezoelectric Actuator, Active Vibration Control, Mounting System

1* School of Mechanical Engineering, Yeungnam University
E-mail: bikim@yu.ac.kr

1. Introduction

Engine mounting system is a vibration isolator between the engine and the chassis. In the days of lightweight and efficient vehicles, increasing the excitation force of the engine generates enormous amount of vibrations which may seriously cause the riding feeling to people[1]. In order to solve this problem, a lot of research on engine mounting systems have been conducted.

PZT actuators are usually applied to conduct active mounting systems and previous studies showed that the PZT-type active engine mount has a very good isolation performance and can reduce vibration at both lower and higher frequencies[2]. The PZT stack actuators are also integrated into the struts of the aircraft engine mount system. Numerical modeling and analysis were carried out and the performance showed the effectiveness of vibration control[3]. Active vibration control with structure-actuator-interaction (SAI) for a flexible plate structure is constructed according to magneto-mechanical coupling. The experimental results show that the stiffness effect of the plate structure could be increased and the amplitudes of the plate vibration are reduced[4]. Secondary forces generated by the actuators rely on a control signal from algorithm implemented with a real-time DSP to reduce unwanted vibration. Er-MCSI algorithm is compared with the FX-LMS algorithm which are applied to active mount fitted to a saloon car equipped with a four-cylinder turbo-diesel engine. Both algorithms reduced 50-90% of vibration under normal driving conditions[5].

Also, many studies are devoted on the location of engine mounts for vibration reduction. The optimal locations and orientation angles of each engine mount are determined by using a dynamic optimization process to achieve the minimum mean force transmissibility [6]. The excitation force of an operating engine from the acceleration data measured at the mounting points are derived from the dynamic deformation of the engine support. The results showed the best position of powertrain mounts to reduce vibrations transmitted to the chassis by three uncoupling techniques[7]. A study on vibration attributes of heavy commercial vehicles are conducted with respect to different engine mount positions. The results showed how the engine isolation can also be altered by location of the engine isolator along the longitudinal direction of the powertrain[8]. The optimal locations of PZT actuator and sensor are found with genetic algorithm (GA) in a simply supported elastic plate and this research showed the efficiency of GA for these optimization problems[9]. Optimal placement of piezo-patches on a simply supported square plate are determined by modified control matrix and singular value decomposition approach. It is observed that when ten actuators are symmetric about the plate center axes, given greater vibration

suppression can be given[10].

The vibration reduction for coupled-path structures with piezoelectric stack actuators and rubber mounts are studied and the quantification of the active path interaction owing to the dynamic characteristics of the passive system has been conducted. The simulation and experimental results showed that some vibration isolation can be obtained [11]. However, under the same excitation, the effect on vibration reduction can be varied by different locations of active mounts. This study will concentrated on the optimized placement of the active mounting system with simulation.

In this study, an experimental setup shown in Fig. 1 is made for simulating the active mounting system. The upper beam stands for a vehicle engine and the lower beam represents the sub-frame. Between the beams, there are two paths consisting of a piezoelectric stack actuator and a rubber mount to provide active vibration isolation. Based on this setup, this article would carry out the followings; 1) A lumped parameter model is proposed for the given structure and equations of motion are established, and 2) Simulations are conducted and results are analysed to determine a criteria for selecting optimized location of the mounting system.

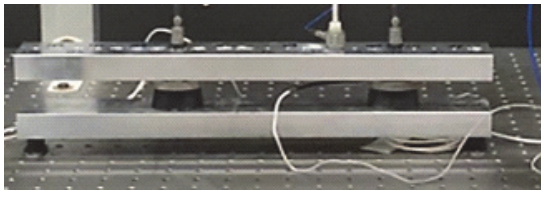

Fig. 1 Experimental setup

2. Mathematical Modeling and Control Force

A lumped parameter model and its free body diagram are shown in Fig. 2. Here, m_s, m_r and I_{sy}, I_{ry} are the mass of beams and their moment of inertia for y axis. $l_{1,2}$, $l_{r1,2}$ are the length between locations and θ_{sy}, θ_{ry} are rotational motions of each beam. k_{mi}, k_{bri} are the real stiffness and ϵ_is are vertical motions. $F_1(t)$, $F_2(t)$ and $F(t)$ are the control forces and disturbance force. d is the distance between disturbance and center of bar on the upper beam.

All the parameters above are determined

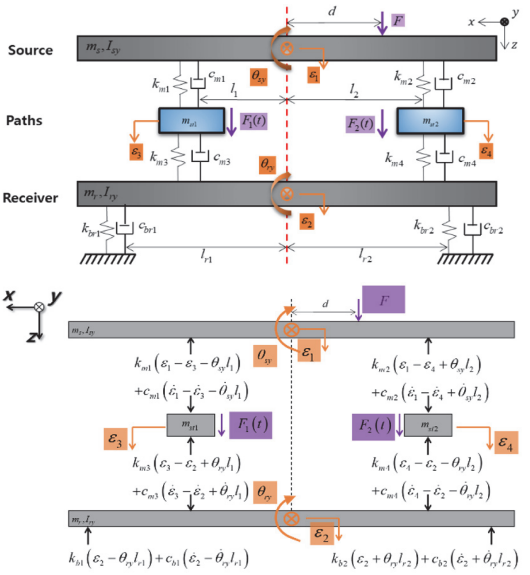

Fig. 2 6-DOF lumped parameter model and free body diagram

based on the measured data from the experimental setup shown in Fig. 1.

Here, $\boldsymbol{M,K,C}$ are inertia, complex valued stiffness, and damping matrix, respectively. Also, $\boldsymbol{q}(t)$, $\boldsymbol{F}(t)$, $\boldsymbol{W}(t)$ are displacement, control force, and disturbance force vector, respectively.

$$\boldsymbol{M}\ddot{\boldsymbol{q}}(t)+\boldsymbol{C}\dot{\boldsymbol{q}}(t)+\boldsymbol{K}\boldsymbol{q}(t)=\boldsymbol{F}(t)+\boldsymbol{W}(t) \quad (1)$$

$$\boldsymbol{M}=diag(\{m_s\ m_r\ m_{st1}\ m_{st2}\ I_{sy}\ I_{ry}\}) \quad (2)$$

$$\boldsymbol{W}(t)=\{(F(t)\ 0\ 0\ 0\ F(t)d_1\ 0)\}^T \quad (3a)$$

$$\boldsymbol{F}(t)=\{0\ 0\ F_1(t)\ F_2(t)\ 0\ 0\}^T \quad (3b)$$

$$\boldsymbol{q}(t)=\{\varepsilon_1\ \varepsilon_2\ \varepsilon_3\ \varepsilon_4\ \theta_{sy}\ \theta_{ry}\}^T \quad (3c)$$

Assuming complex valued variable for control forces F_1, F_2 and the disturbance force F, the dynamic stiffness matrix is defined as $\tilde{\boldsymbol{\kappa}}=[-\omega^2\boldsymbol{M}'+\boldsymbol{K}']^{-1}$. According to formula $\boldsymbol{H}^{*'}=[\boldsymbol{\kappa}']^{-1}$, complex valued compliance matrix $\boldsymbol{H}^{*'}$ can be obtained and then, the phase-matching method is used to eliminate the phase difference caused by disturbance force and control force[4]. With this method, the motions should be reduced to virtually zero and an equation can be established for finding control force, as shown below.

3. Simulation Results and Analysis

Actuator 1 (active mount on the left side of the beam) and actuator 2 (active mount on the right side of the beam) are placed on both sides of the beam and the shaker is installed on the right side of the beam ($40 \le S \le P$). The shaker is fixed at a certain point and the actuator 1 and actuator 2 are placed from near center of the beam to the end edges of the beam ($21 \le A_1 \le P$, $21 \le A_2 \le P$). According to the positions of two actuators, the force and phase in each path is calculated and analysed by 3D plots as follows.

Fig. 4(a) shows the force of path 1 when the shaker is located at 140 mm from the center. The simulation results show that minimum force on the path 1 is required

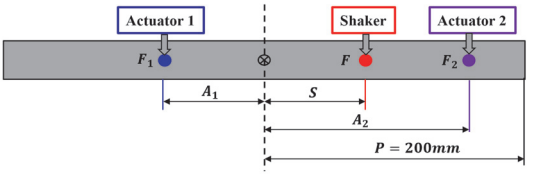

Fig. 3 Dimensions of target system

$$\boldsymbol{K}=\begin{bmatrix} k_{m1}+k_{m2} & 0 & -k_{m1} & -k_{m2} & k_{m2}l_2-k_{m1}l_1 & 0 \\ 0 & k_{m3}+k_{m4}+k_{b1}+k_{b2} & -k_{m3} & -k_{m4} & 0 & k_{m4}l_2-k_{m3}l_1+k_{b2}l_{r2}-k_{b1}l_{r1} \\ -k_{m1} & -k_{m3} & k_{m1}+k_{m3} & 0 & k_{m1}l_1 & k_{m3}l_1 \\ -k_{m2} & -k_{m4} & 0 & k_{m2}+k_{m4} & -k_{m2}l_2 & -k_{m4}l_2 \\ k_{m2}l_2-k_{m1}l_1 & 0 & k_{m1}l_1 & -k_{m2}l_2 & k_{m1}l_1^2+k_{m2}l_2^2 & 0 \\ 0 & k_{m4}l_2-k_{m3}l_1+k_{b2}l_{r2}-k_{b1}l_{r1} & k_{m3}l_1 & -k_{m4}l_2 & 0 & k_{m3}l_1^2+k_{m4}l_2^2+k_{b1}l_{r1}^2+k_{b2}l_{r2}^2 \end{bmatrix} \quad (4)$$

$$\boldsymbol{C}=\begin{bmatrix} c_{m1}+c_{m2} & 0 & -c_{m1} & -c_{m2} & c_{m2}l_2-c_{m1}l_1 & 0 \\ 0 & c_{m3}+c_{m4}+c_{b1}+c_{b2} & -c_{m3} & -c_{m4} & 0 & c_{m4}l_2-c_{m3}l_1+c_{b2}l_{r2}-c_{b1}l_{r1} \\ -c_{m1} & -c_{m3} & c_{m1}+c_{m3} & 0 & c_{m1}l_1 & c_{m3}l_1 \\ -c_{m2} & -c_{m4} & 0 & c_{m2}+c_{m4} & -c_{m2}l_2 & -c_{m4}l_2 \\ c_{m2}l_2-c_{m1}l_1 & 0 & c_{m1}l_1 & -c_{m2}l_2 & c_{m1}l_1^2+c_{m2}l_2^2 & 0 \\ 0 & c_{m4}l_2-c_{m3}l_1+c_{b2}l_{r2}-c_{b1}l_{r1} & c_{m3}l_1 & -c_{m4}l_2 & 0 & c_{m3}l_1^2+c_{m4}l_2^2+c_{b1}l_{r1}^2+c_{b2}l_{r2}^2 \end{bmatrix} \quad (5)$$

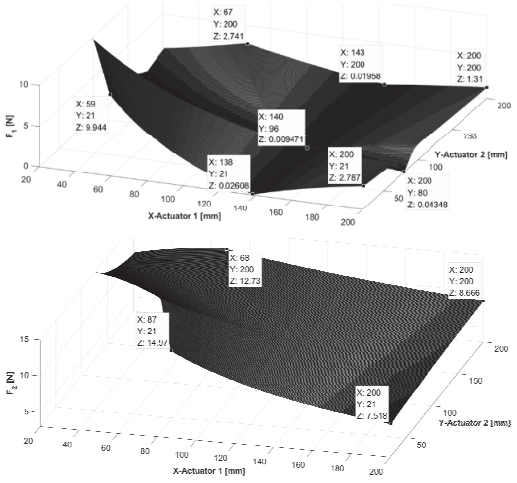

Fig. 4 Control force of path 1 and path 2 when the ED shaker is installed at 140 mm

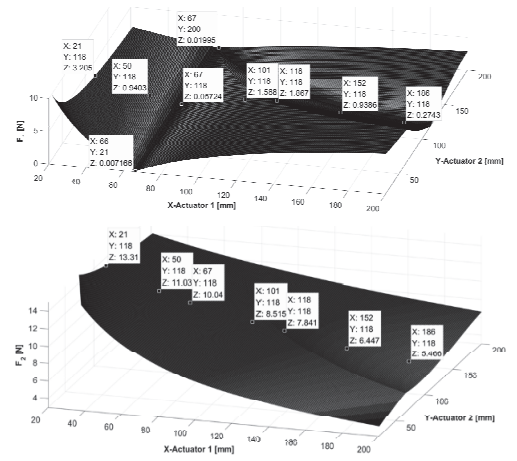

Fig. 5 Control force of path 1 and path 2 when the ED shaker is installed at 67 mm

when the actuator 1 is located at around 138 mm from the center. This means that one actuator should be placed at almost exactly the opposite symmetry of the shaker. Also, no matter how the position of actuator 2 changes, it has no effect on the result.

Fig. 4(b) shows the force of path 2 and regardless of the position of actuator 2, it appears that path 2 becomes smaller when actuator 1 gets closer to the end of the beam. Since the distance between the actuator 2 and the shaker is smaller than the distance between the actuator 1 and the shaker (the actuator 2 and the shaker on the same side), it can be seen that control force needed on path 2 is much larger than path 1. So, considering the size of piezoelectric stack actuator, it is easier to control path 2 than path 1 and the specification of the actuator should be determined with respect to the required force on path 2.

Similar tendency can be seen from the case when the shaker is installed at 67 mm from the center. Below table is the control forces needed on path 1 and path 2 when the shaker is fixed at 67 mm and the actuator 2 is installed at 118 mm, arbitrarily.

$$\boldsymbol{H}^{*'} = \begin{bmatrix} H_{11}^{*'} & H_{12}^{*'} & H_{13}^{*'} & H_{14}^{*'} & H_{15}^{*'} & H_{16}^{*'} \\ H_{21}^{*'} & H_{22}^{*'} & H_{23}^{*'} & H_{24}^{*'} & H_{25}^{*'} & H_{26}^{*'} \\ H_{31}^{*'} & H_{32}^{*'} & H_{33}^{*'} & H_{34}^{*'} & H_{35}^{*'} & H_{36}^{*'} \\ H_{41}^{*'} & H_{42}^{*'} & H_{43}^{*'} & H_{44}^{*'} & H_{45}^{*'} & H_{46}^{*'} \\ H_{51}^{*'} & H_{52}^{*'} & H_{53}^{*'} & H_{54}^{*'} & H_{55}^{*'} & H_{56}^{*'} \\ H_{61}^{*'} & H_{62}^{*'} & H_{63}^{*'} & H_{64}^{*'} & H_{65}^{*'} & H_{66}^{*'} \end{bmatrix} \quad \begin{Bmatrix} F_1 \\ F_2 \end{Bmatrix} = \frac{F}{\left|H_{13}^{*'}\right|\left|H_{24}^{*'}\right| - \left|H_{14}^{*'}\right|\left|H_{23}^{*'}\right|} \begin{Bmatrix} \left|H_{14}^{*'}\right|\left|H_{21}^{*'} + dH_{25}^{*'}\right| - \left|H_{24}^{*'}\right|\left|H_{11}^{*'} + dH_{15}^{*'}\right| \\ \left|H_{23}^{*'}\right|\left|H_{11}^{*'} + dH_{15}^{*'}\right| - \left|H_{13}^{*'}\right|\left|H_{21}^{*'} + dH_{25}^{*'}\right| \end{Bmatrix} \tag{6}$$

$$F_1 = F\left(\frac{\left|H_{14}^{*'}\right|\left|H_{21}^{*'}+dH_{25}^{*'}\right| - \left|H_{24}^{*'}\right|\left|H_{11}^{*'}+dH_{15}^{*'}\right|}{\left|H_{13}^{*'}\right|\left|H_{24}^{*'}\right| - \left|H_{14}^{*'}\right|\left|H_{23}^{*'}\right|}\right) \qquad F_2 = F\left(\frac{\left|H_{23}^{*'}\right|\left|H_{11}^{*'}+dH_{15}^{*'}\right| - \left|H_{13}^{*'}\right|\left|H_{21}^{*'}+dH_{25}^{*'}\right|}{\left|H_{13}^{*'}\right|\left|H_{24}^{*'}\right| - \left|H_{14}^{*'}\right|\left|H_{23}^{*'}\right|}\right) \tag{7}$$

Table 1. Control forces of path 1 and path 2 (Shaker at 67 mm and Actuator 2 at 118 mm)

Actuator 1 [mm]	Path 1 [N]	Path 2 [N]
27	3.25	13.5
50	0.94	11.7
67	0.03	10.6
84	0.93	9.76
101	1.66	9.03
118	1.92	8.32
135	1.35	7.51
152	0.86	6.84
169	0.43	6.29
186	0.35	5.83

4. Conclusion

The simulation results for the 6 DOF beam structure are as follows; (1) Actuator 1 should be placed at almost exactly the opposite symmetry of the shaker and then the force of path 1 would be smallest, no matter how the position of the actuator 2 changes, (2) The force of path 2 becomes smaller when the actuator 1 is located away from the center of gravity of the beam, regardless of the position of the actuator 2. Then, the force of path 2 would be the smallest when the actuator is at the end edge of the beam.

Acknowledgement

This work was supported by the Basic Science Research Program through the National Research Foundation of Korea (NRF), funded by the Ministry of Education (NRF-2021R1A6A1A03039493 and NRF-2022R1F1A1076089).

References

[1] B. Kim, “Powertrain Surface Radiated Noise Analysis using Passive Patches,” Journal of the Korean Society of Industry Convergence, 24(2_1), 111-116, (2021).

[2] L. Sui, X. Xiong, and G. Shi, “Piezo- electric Actuator Design and Application on Active Vibration Control,” 2012 International Conference on Solid State Devices and Materials Science, Physics Procedia 25, 1388-1396, (2012).

[3] M. P. Vijayakumar, U. Ashwin, and S. Raja, “Active Vibration Control of Engine Mount System of Transport Aircraft using PZT Stack Actuators,” Journal of Mechatronics, 2, 226-231, (2014).

[4] J. Jiang, W. Gao, L. Wang, Z. Teng, and Y. Liu, “Active vibration control based on modal controller considering structure- actuator interaction,” Journal of Mecha- nical Science and Technology, 32 (8), 3515-3521, (2018).

[5] A. J. Hillis, A. J. L. Harrison, and D. P. Stoten, “A comparison of two adaptive algorithms for the control of active engine mounts,” Journal of Sound and Vibration, 286, 37–54, (2005).

[6] L. Ooi, and Z. M Ripin, “Optimization of an engine mounting system with consideration of frequency dependent stiffness and loss factor,” Journal of Vibration and Control, 22(10), 2406-2419, (2016).

[7] A. E. Hafidi, B. Martin, A. Loredo, and E. Jego, “Vibration reduction on city buses: Determination of optimal position of engine mounts,” Mechanical Systems and Signal Processing, 24(7), 2198-2209, (2010).

[8] M. N. Kumar, K. Chinnaraj, and E. Loganathan, "Study of Effect of Varying Engine Mount Locations and Stiffness on Vibration in Heavy Commercial Vehicles," International Journal of Engineering Research and Technology, 3(2), 2765-2768, (2014).

[9] I. Bruant, L. Gallimard, and S. Nikoukar, "Optimal piezoelectric actuator and sensor location for active vibration control using genetic algorithm," Journal of Sound and Vibration, 329(10), 1615-1635, (2010).

[10] D. Chhabra, G. Bhushan, and P. Chandna, "Multilevel optimization for the placement of piezo-actuators on plate structures for active vibration control using modified heuristic genetic algorithm," Proc. SPIE 9050, Industrial and Commercial Applications of Smart Structures Technologies, (2014).

[11] J. Liette, J. T. Dreyer, and R. Singh, "Interaction between two active structural paths for source mass motion control over mid-frequency range," Journal of Sound and Vibration, 333, 2369-2385, (2014).

(Manuscript received June 28, 2022;
revised August 09, 2022; accepted August 10, 2022)